Three-Dimensional Supramolecular Organization of Molecular Rods Depending on Coil Cross Section in Rod−Coil Molecules

Byoung-Ki Cho,*,† Yeon-Wook Chung,† and Myongsoo Lee*,‡

Department of Chemistry, Dankook University, 147, Hannam-ro, Yonsan-gu, Seoul 140-714, Korea, and Center for Supramolecular Nano-Assembly and Department of Chemistry, Yonsei University, Seoul 120-749, Korea

Received August 29, 2005; Revised Manuscript Received September 20, 2005

ABSTRACT: Coil−rod−coil molecules were prepared to have identical coil volume fraction ($f = 0.78$) relative to mesogenic rod segment, but different coil segments, i.e., poly(propylene oxide) with DP = 13 and poly(ethylene oxide) with DP = 18. Their self-assembly behavior in the solid and liquid crystalline phases was investigated using optical polarized microscopy and small-angle X-ray scattering techniques. The coil−rod−coil molecule with the poly(propylene oxide) coils shows a 3-D body-centered tetragonal micellar structure in both solid and liquid crystalline phases. In contrast, the coil−rod−coil molecule with the poly(ethylene oxide) coils exhibits a 3-D honeycomb-like lamellar structure in both solid and liquid crystalline phases. These results demonstrate that the cross-sectional area of coil significantly influences the self-assembly behavior of rod segments even at constant coil volume fraction relative to rod segment and provides the way to fine-tune 3-D supramolecular structures in the rod−coil system.

Introduction

Rod−coil molecules consisting of elongated rigid rod and flexible coil have been attracted as interesting self-assembling soft materials due to the creation of novel functional materials by combination of their self-assembling capability and functional uniqueness.[1] For the decade, the experimental efforts have been tried to prove the self-assembly behavior of the rod−coil system.[2] As proposed by the early theoretical works, the coil volume fraction in the rod−coil system has been considered as the main molecular parameter to determine self-assembled nanostructures.[3] Experimentally, it has been demonstrated that the systematic variation of coil length (i.e., coil volume fraction) in AB diblock rod−coil molecules gives rise to a variety of supramolecular architectures ranging form lamellar to hexagonal columnar structures with a continuous cubic structure as the intermediate regime.[4] Besides the coil volume fraction, we have recently investigated the dependence of assembled structure upon the rod length at constant coil volume fraction in coil−rod−coil molecules and proved that large anisotropy of rod building block significantly shifts the supramolecular structure toward more continuous domain structures even at constant coil volume fraction.[5]

The present paper describes the opposite way to modulate the supramolecular structure, which varies only the coil structure but maintaining rod segment constant. We report on the influence of cross-sectional area of coil segment upon the self-assembly behavior of rod−coil system. To this end, ABA type coil−rod−coil molecules were prepared to have identical coil volume fraction ($f = 0.78$) relative to mesogenic rod segment, but different coil segments, i.e., poly(propylene oxide) and poly(ethylene oxide), respectively (Figure 1). Compared to poly(propylene oxide) coil, poly(ethylene oxide) coil has a smaller cross-sectional area by lack of a lateral methyl group. In this rational approach for a constant coil volume fraction, the influence of coil cross section on the rod packing structure can be explained.

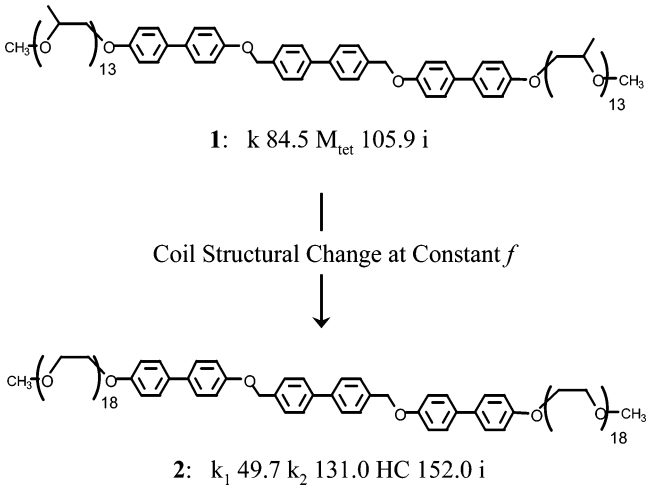

Figure 1. Molecular structure and phase transition temperatures of coil−rod−coil molecules **1** and **2**. Temperatures are given in °C; k: crystalline; M_{tet}: body-centered tetragonal micellar; HC: honeycomb-like lamellar; i: isotropic.

Experimental Section

Materials. Monomethylated poly(ethylene glycol) coils (DP = 7, 14, 18, and 23) from Aldrich were used as received. 4,4′-Biphenol (99%), 4-hydroxy-4′-biphenylcarboxylic acid (98%), toluene-*p*-sulfonyl chloride (98%), and bis(bromomethyl)biphenyl (99%) from Tokyo Kasei were used as received. Dichloromethane was dried by distillation from calcium hydride and stored over type 4 Å molecular sieve. Pyridine was dried by distillation from sodium metal and stored over type 4 Å molecular sieve.

Synthesis. Compound **2** was synthesized by etherification of 4-oxy-4′-phenylphenol-terminated poly(ethylene oxide) coil with 4,4′-bis(bromomethyl)biphenyl.[6] The synthesis of compounds **3**−**5** was performed by esterification of appropriate 4-oxy-4′-biphenylcarboxylic acid-terminated poly(ethylene oxide)s with 4,4′-biphenol.[4]

† Dankook University.
‡ Yonsei University.
* To whom correspondence should be addressed. E-mail: chobk@dankook.ac.kr or mslee@yonsei.ac.kr.

10.1021/ma051890b CCC: $30.25
Published on Web 11/03/2005

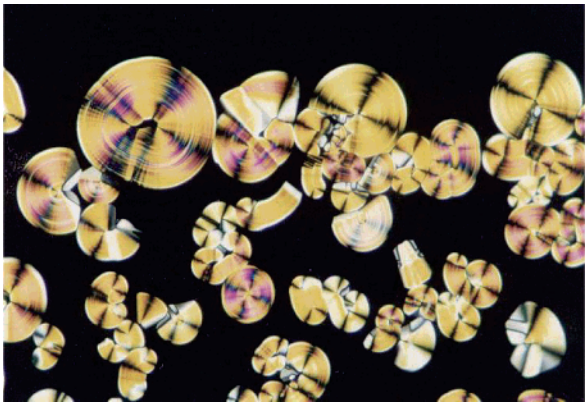

Figure 2. Optical polarized micrograph (100×) of the texture exhibited by the 3-D honeycomb-like lamellar liquid crystalline phase of **2** at the transition from the isotropic liquid phase at 149 °C.

Table 1. Small-Angle X-ray Diffraction Data for 3-D Hexagonal Structure of 2 in the k_2 Crystalline Phase[a]

h	*k*	*l*	q_{obsd} (nm^{-1})	q_{calcd} (nm^{-1})
0	0	2	0.761	0.761
1	0	1	0.953	0.953
1	0	3	1.431	1.437
1	1	0	1.513	1.514
2	0	0	1.750	1.748
1	0	4	1.750	1.755
2	0	2	1.893	1.906
0	0	6	2.282	2.283

[a] q_{obsd} and q_{calcd} are the scattering vectors of the observed reflections (Figure 3a) and calculated for the 3-D hexagonal structure (*P*6$_3$/*mmc* space group symmetry) with lattice parameters $a = 8.3$ and $c = 16.5$ nm.

2: Yield 67%. ^{1}H NMR (250 MHz, $CDCl_3$, δ, ppm): 7.45−7.65 (m, 16Ar−H, *m* to OCH_2phenyl, *m* to OCH_2CH_2, *o* to CH_2Ophenyl and *m* to CH_2Ophenyl), 6.95−7.07 (m, 8Ar−H, *o* to OCH_2phenyl, *o* to OCH_2CH_2), 5.14 (s, 4H, OCH_2phenyl), 3.54−4.16 (m, 144H, OCH_2CH_2), 3.38 (s, 6H, CH_3O). Anal. Calcd for $C_{112}H_{178}O_{40}$: C, 62.15; H, 8.29. Found: C, 62.24; H, 8.24. $\bar{M}_w/\bar{M}_n = 1.04$ (GPC).

3: Yield 45%. ^{1}H NMR (250 MHz, $CDCl_3$, δ, ppm): 8.26 (d, 4Ar−H, *o* to COOphenyl, $J = 8.4$ Hz), 7.56−7.72 (m, 12Ar−H, *m* to biphenylcarboxylate, *m* to COOphenyl and *m* to CH_2O), 7.32 (d, 4Ar−H, *o* to biphenylcarboxylate, $J = 8.5$ Hz), 7.03 (d, 4Ar−H, *o* to CH_2O, $J = 8.4$ Hz), 3.52−4.20 (m, 56H, OCH_2CH_2), 3.37 (s, 6H, CH_3O). Anal. Calcd for $C_{68}H_{86}O_{20}$: C, 66.76; H, 7.09. Found: C, 66.30; H, 7.05. $M_w/M_n = 1.11$ (GPC).

4: Yield 47%. ^{1}H NMR (250 MHz, $CDCl_3$, δ, ppm): 8.26 (d, 4Ar−H, *o* to COOphenyl, $J = 8.3$ Hz), 7.56−7.73 (m, 12Ar−H, *m* to biphenylcarboxylate, *m* to COOphenyl and *m* to CH_2O), 7.35 (d, 4Ar−H, *o* to biphenylcarboxylate, $J = 8.5$ Hz), 7.02 (d, 4Ar−H, *o* to CH_2O, $J = 8.4$ Hz), 3.50−4.20 (m, 112H, OCH_2CH_2), 3.37 (s, 6H, CH_3O). Anal. Calcd for $C_{96}H_{142}O_{34}$: C, 62.66; H, 7.78. Found: C, 62.30; H, 7.55. $M_w/M_n = 1.06$ (GPC).

5: Yield 45%. ^{1}H NMR (250 MHz, $CDCl_3$, δ, ppm): 8.27 (d, 4Ar−H, *o* to COOphenyl, $J = 8.5$ Hz), 7.53−7.72 (m, 12Ar−H, *m* to biphenylcarboxylate, *m* to COOphenyl and *m* to CH_2O), 7.33 (d, 4Ar−H, *o* to biphenylcarboxylate, $J = 8.5$ Hz), 7.03 (d, 4Ar−H, *o* to CH_2O, $J = 8.4$ Hz), 3.52−4.22 (m, 184H, OCH_2CH_2), 3.36 (s, 6H, CH_3O). Anal. Calcd for $C_{132}H_{214}O_{52}$: C, 60.21; H, 8.19. Found: C, 60.40; H, 8.03. $M_w/M_n = 1.10$ (GPC).

Techniques. ^{1}H NMR spectra were recorded from $CDCl_3$ solutions on a Bruker AM 250 spectrometer. The purity of the products was checked by thin-layer chromatography (TLC; Merck, silica gel 60). A Perkin-Elmer DSC-7 differential scanning calorimeter equipped with 1020 thermal analysis controller was used to determine the thermal transitions, which were reported as the maxima and minima of their endothermic or exothermic peaks. In all cases, the heating and cooling rates were 10 °C min^{-1}. A Nikon Optiphot 2-pol optical polarized microscopy (magnification: 100×) equipped with a Mettler FP 82 hot stage and a Mettler FP 90 central processor was used to observe the thermal transitions and to analyze the anisotropic texture. Microanalyses were performed with a Perkin-Elmer 240 elemental analyzer at Organic Chemistry Research Center, Seoul, Korea. X-ray scattering measurements were performed in transmission mode with synchrotron radiation at the 3C2 X-ray beamline at Pohang Accelerator Laboratory, Korea. The data were collected in 1-dimensional powder diffraction patterns. To investigate structural changes on heating, the sample was held in an aluminum sample holder which was sealed with the window of 7 μm thick Kapton films on both sides. The sample was heated with two cartridge heaters, and the temperature of the samples was monitored by thermocouple placed close to the sample. Background scattering correction was made by subtracting the scatterings from the Kapton. Molecular weight distributions (M_w/M_n) were determined by gel permeation chromatography (GPC) with a Waters R401 instrument equipped with Styragel HR 3, 4, and 4E columns, M7725i manual injector, column heating chamber, and 2010 Millennium data station. Measurements were made by using an UV detector and $CHCl_3$ as a solvent (1.0 mL min^{-1}).

Table 2. Small-Angle X-ray Diffraction Data for 3-D Hexagonal Structure of 2 in the Liquid Crystalline Phase[a]

h	*k*	*l*	q_{obsd} (nm^{-1})	q_{calcd} (nm^{-1})
0	0	2	0.883	0.883
1	0	1	1.020	1.020
1	1	0	1.609	1.593
1	0	3	1.609	1.615
0	0	4	1.758	1.766

[a] q_{obsd} and q_{calcd} are the scattering vectors of the observed reflections (Figure 3b) and calculated for the 3-D hexagonal structure (*P*6$_3$/*mmc* space group symmetry) with lattice parameters $a = 7.9$ and $c = 14.2$ nm.

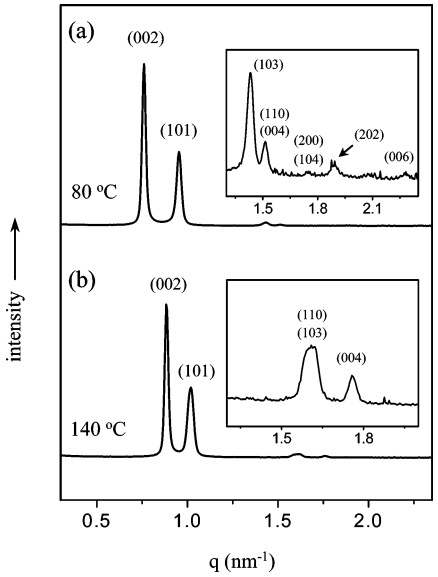

Figure 3. Small-angle X-ray diffraction patterns measured at different temperatures in (a) the honeycomb-like lamellar crystalline phase at 80 °C and (b) honeycomb-like lamellar liquid crystalline phase at 140 °C for **2**.

Results and Discussion

The synthesis of coil−rod−coil molecule **1** was reported elsewhere, and **2** was synthesized by following a similar stepwise procedure.[6] The final coil−rod−coil molecules were characterized by ^{1}H NMR and elemental analysis, and their results are in good agreement with

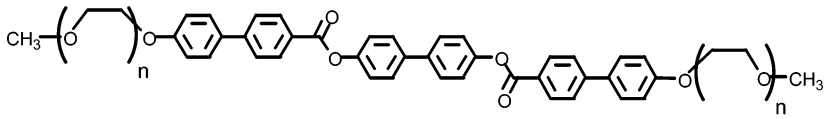

3: n = 7 k_1 46.7 k_2 148.9 s_C 220.5 i

4: n = 14 k_1 53.9 k_2 137.7 OI 147.7 i

5: n = 23 k_1 63.1 k_2 121.5 i

Figure 4. Molecular structure and thermal behavior of **3**−**5**. The transition temperatures obtained from heating scan are given in °C; k: crystalline; s_C: smectic C; OI: optically isotropic liquid crystalline; i: isotropic liquid phase.

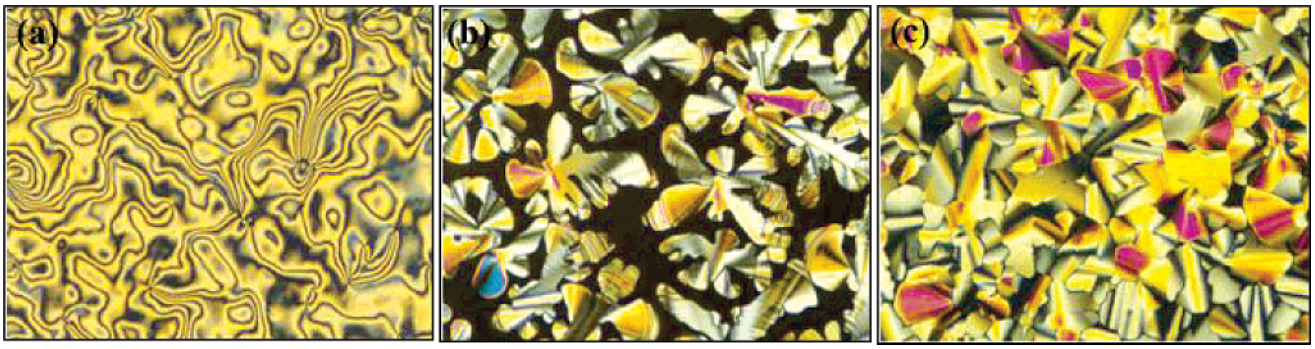

Figure 5. Representative optical micrographs (100×) of (a) the texture exhibited by the s_C mesophase of **3** at 200 °C, (b) the growing texture of the honeycomb-like lamellar k_2 phase at the transition from the optically isotropic mesophase of **4** at 133 °C, and (c) the texture of the hexagonal columnar k_2 crystalline of **5** at 117 °C on cooling scan.

the expected molecular structures. Their polydispersities (M_w/M_n) from gel permeation chromatography (GPC) were found to be less than 1.05, indicative of narrow molecular weight distributions. Their thermal behavior was determined by differential scanning calorimetry (DSC) measurements and polarized optical microscopy (POM) observations as summarized in Figure 1. Coil−rod−coil molecule **1** with PPO segments shows only a crystalline melting transition associated with rod segments. Coil−rod−coil molecule **2** with PEO segments, however, shows two crystalline states designated as k_1 and k_2. In the former k_1 state, both rod and PEO coil segments can be considered to be crystalline, while only rod segments to be crystalline in the latter k_2 state. After melting of rod segments, both molecules show the isotropic disordering transitions, suggestive of the existence of a liquid crystalline phase.

The X-ray diffraction and optical polarized microscopic observations of **1** were reported previously and have shown that **1** containing the PPO coils self-organizes into a 3-D body-centered tetragonal lattice, composed of the organized rod bundles and PPO coil matrix in both solid and mesophase (Figure 7).[6]

In contrast, **2** shows significantly distinct self-assembly behavior. On the basis of POM investigation, dendritic domains with striations that merge into an arced pseudofocal conic texture are exhibited on slow cooling from isotropic liquid phase (Figure 2). Furthermore, this texture is maintained in the k_2 state without abrupt change. This optical microscopic observation is strongly suggestive of a lamellar structure with hexagonally ordered coil perforations.[5,7] To characterize the microstructures, small-angle X-ray scattering (SAXS) experiments were performed with elevation of temperature. In the k_2 state at 80 °C, the SAXS pattern shows a number of well-resolved reflections. They can be indexed as a 3-dimensional hexagonal order ($P6_3/mmc$ symmetry) with cell parameters a = 8.3 nm and c = 16.5 nm (Figure 3a and Table 1). In the mesophase at 140 °C, SAXS data show the analogous reflections to that in k_2 state, interpreted as a 3-D hexagonal structure with unit cell dimensions of a = 7.9 nm and c = 14.2 nm (Figure 3b and Table 2). As shown in the powder X-ray patterns of Figure 3, the (hkl) reflections with nonzero l values were dominantly observed.[8] In addition, the peak intensity associated with the (002) reflecton is the most intense, suggesting that the fundamental structure is lamellar.[9] On the basis of the POM observation and the SAXS data including the peak

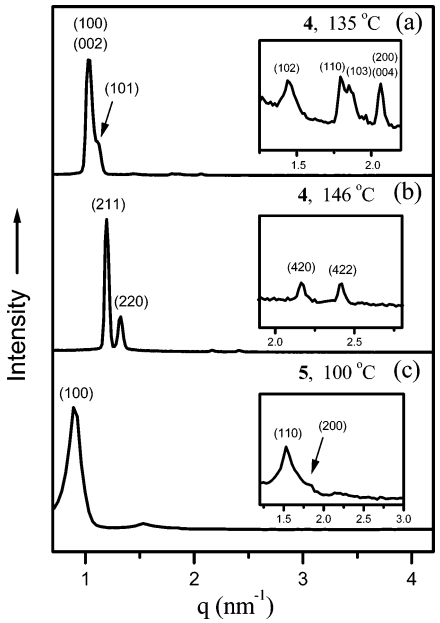

Figure 6. Small-angle powder X-ray diffraction patterns measured in (a) the honeycomb-like lamellar crystalline phase at 135 °C, (b) the gyroid mesophase at 146 °C for **4**, and (c) the hexagonal columnar crystalline phase at 100 °C for **5**.

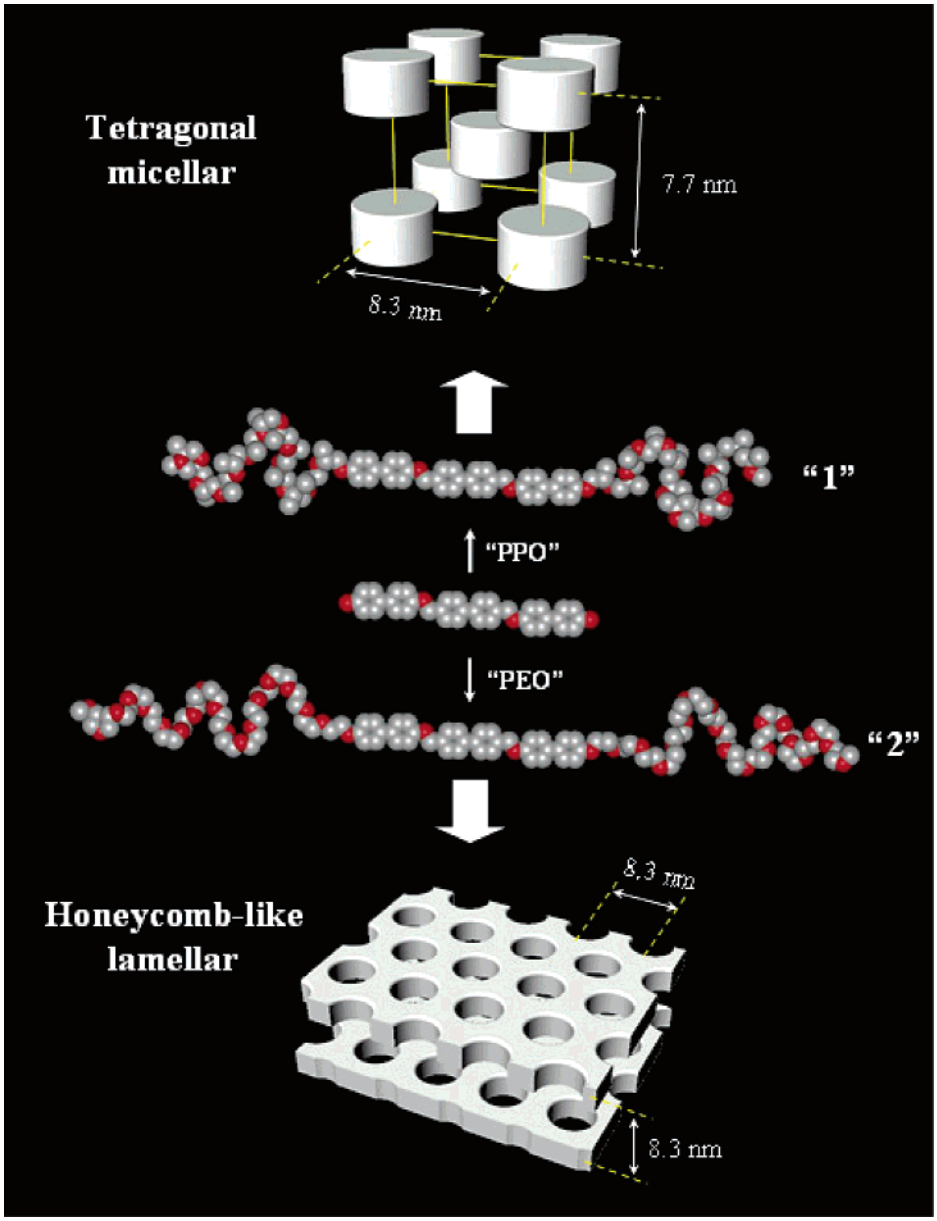

Figure 7. Coil cross-section-dependent self-organization of rod−coil molecules **1** and **2** at constant coil volume fraction and rod segment. For clarity, two AB stacked layers are presented in the honeycomb-like lamellar structure, and the depicted interlayer distance is a half of the lattice parameter *c*. Also, structural models on the upper and lower omit the coil parts.

patterns and intensities, the supramolecular structures in both crystalline and mesophases might be a honeycomb-like lamellar structure where hexagonally perforated layers stacked in ABAB order (Figure 7).

To corroborate the identity of the honeycomb-like lamellar structure of **2**, we investigated the phase behavior of a series of homologous coil−rod−coil molecules **3**−**5** as a function of PEO coil length (Figure 4). The rod segment of **3**−**5** consists of three biphenyl groups with two ester linkages which is nearly identical to the rod segment of **1** and **2** in terms of rod composition and length. (From CPK models, both are calculated to be 30 Å.) Therefore, the above argument can be rationalized by comparing the phase behavior of **2** with those of **3**−**5** series. As expected for molecules based on rodlike mesogens, **3** with the shortest PEO coils exhibits a lamellar k_2 crystalline and a smectic C liquid crystalline phases (Figure 5a).

In contrast, **4** with the intermediate PEO coils shows a honeycomb-like lamellar structure ($P6_3/mmc$ symmetry) with lattice parameters of $a = 7.0$ nm and $c = 12.2$ nm in the k_2 state, similar to the k_2 crystalline structure in **2** (Figures 5b and 6a). In addition, **4** displays an optically isotropic mesophase. In the mesophase, the X-ray scattering data show four peaks with q-spacing ratios of $\sqrt{6}$, $\sqrt{8}$, $\sqrt{20}$, and $\sqrt{24}$, which can be indexed as (211), (220), (420), and (422) reflections of a gyroid structure (Figure 6b). From the previous block copolymer study, it is well-known that perforated lamellar and gyroid structures appear at nearly identical volume fraction.[10] Therefore, the mesophase behavior of **2** and **4** with the similar PEO coil lengths seems to be reasonable. Upon further increase of PEO coil length, **5** with the longest PEO coils shows a hexagonal columnar k_2 crystalline phase, the lattice parameter of which was estimated to be 8.0 nm from SAXS data (Figures 5c and 6c), but any liquid crystalline phase is not shown. Considering the observed phase behavior of **2**−**5** molecules in particularly the k_2 state and the phase window of the rod−coil system as a function of coil

Table 3. Characterization of the Coil−Rod−Coil Molecules in k_2 Crystalline State by Small-Angle X-ray Scattering[a]

			lamellar	honeycomblike lamellar				hexagonal columnar	teragonal micellar		
molecule	DP of PEO	stretched molecular length *l* (nm)	interlayer distance (nm)	lattice parameter (nm) *a*	lattice parameter (nm) *c*	perforation diam (nm)	interlayer distance (nm)	interccolumn distance *a* (nm)	lattice parameter (nm) *a*	lattice parameter (nm) *c*	rod bundle diam (nm)
1		10.0							8.3	7.7	5.0
2	18	12.2		8.3	16.5	5.4	8.3				
3	7	6.6	5.8								
4	14	10.2		7.0	12.2	4.7	6.1				
5	23	14.6						8.0			

[a] The interlayer distance in the honeycomb-like lamellar structure is a half of lattice parameter *c* because of the ABAB stacking mode of perforated layers.

length,[4] the identity of the honeycomb-like lamellar structure in **2** with the PEO coils (DP = 18) is pronounced because the columnar structure with higher interfacial area is observed from **5** based on a higher coil volume fraction (Table 3). In addition, comparing ratios of interlayer (in honeycomb-like lamellar) or intercolumn (in hexagonal columnar) distances with respect to stretched molecular length argues for the above interpretation because the ratio gives a clue for how much coils in a given structure are stretched. Since coils in structures closer to layered structure are more stretched, the ratios will be larger. The ratios in the honeycomb-like lamellar structures of **2** and **4** were estimated to be 0.68 and 0.60; on the other hand, the ratio in the hexagonal columnar structure of **5** is 0.55 (Table 3). Therefore, the basic structures of **2** and **4** can be considered to be lamellar rather than micellar.

The different self-assembly behavior of **1** and **2** with identical coil volume fraction ($f = 0.78$) points out the significance of coil cross-sectional area for the packing of rod segments. It can be rationalized by the consideration of coil density at rod/coil interface dependent upon coil cross section. For a given space at rod/coil junction, the coils with larger cross-sectional area cause more space crowding. The steric repulsion resulted from the space crowding leads to the stretched conformation of coils, leading to the coil stretching penalty.[3] The morphological transition from continuous (in this study the honeycomb-like lamellar structure of **2**) into discrete rod packing structures (in this study the tetragonal structure of **1**) allows coils enough room to lower the coil conformational energy.

In summary, we have observed that self-assembled 3-D supramolecular structure changes significantly from a continuous honeycomb-like rod packing structure to discrete rod bundles in a coil matrix as a function of coil cross-sectional area at constant coil volume fraction. These results demonstrate that self-assembly of rods can be fine-tuned in 3-D nanospace since, in addition to coil volume fraction, coil cross section is an independent parameter to build a variety of supramolecular structures.

Acknowledgment. This work was supported by the National Creative Research Initiative Program of the Korean Ministry of Science and Technology. We are grateful to Pohang Accelarator Laboratory, Korea, for using Synchrotron Radiation Source and D.-W. Jang for help with the synthesis of coil−rod−coil molecules **3**−**5**.

References and Notes

(1) Lee, M.; Cho, B.-K.; Zin, W.-C. *Chem. Rev.* **2001**, *101*, 3869−3892.
(2) (a) Chen, J. T.; Thomas, E. L.; Ober, C. K.; Mao, G.-p. *Science* **1996**, *273*, 343−346. (b) Stupp, S. I.; Lebonheur, V.; Walker, K.; Li, L. S.; Huggins, K. E.; Keser, M.; Amstutz, A. *Science* **1997**, *276*, 384−389. (c) Zubarev, E. R.; Pralle, M. U.; Li, L.; Stupp, S. I. *Science* **1999**, *283*, 523−526. (d) Klok, H.-A.; Langenwalter, J. F.; Lecommandoux, S. *Macromolecules* **2000**, *33*, 7819−7826. (e) Jenekhe, S. A.; Chen, X. L. *Science* **1998**, *279*, 1903−1907. (f) Widawski, G.; Rawiso, M.; Francois, B. *Nature (London)* **1994**, *369*, 387−389. (g) Ludwigs, S.; Krausch, G.; Reiter, G.; Losik, M.; Antonietti, M.; Schlaad, H. *Macromolecules* **2005**, *38*, 7532−7535.
(3) Williams, D. R. M.; Fredrickson, G. H. *Macromolecules* **1992**, *25*, 3561−3568.
(4) Lee, M.; Cho, B.-K.; Kim, H.; Yoon, J.-Y.; Zin, W.-C. *J. Am. Chem. Soc.* **1998**, *120*, 9168−9179.
(5) Cho, B.-K.; Lee, M.; Oh, N.-K.; Zin, W.-C. *J. Am. Chem. Soc.* **2001**, *123*, 9677−9678.
(6) Lee, M.; Cho, B.-K.; Jang, Y.-G.; Zin, W.-C. *J. Am. Chem. Soc.* **2000**, *122*, 7449−7455.
(7) Kim, J.-K.; Hong, M.-K.; Ahn, J.-H.; Lee, M. *Angew. Chem., Int. Ed.* **2005**, *44*, 328−332.
(8) Loo, Y.-L.; Register, R. A.; Adamson, D. H.; Ryan, A. J. *Macromolecules* **2005**, *38*, 4947−4949.
(9) (a) Oh, N.-K.; Zin, W.-C.; Im, J.-H.; Ryu, J.-H.; Lee, M. *Chem. Commun.* **2004**, 1092−1093. (b) Jin, L. Y.; Bae, J.; Ahn, J.-H.; Lee, M. *Chem. Commun.* **2005**, 1197−1199.
(10) Khandpur, A. K.; Förster, S.; Bates, F. S.; Hamley, I. W.; Ryan, A. J.; Bras, W.; Almdal, K.; Mortensen, K. *Macromolecules* **1995**, *28*, 8796−8806.

MA051890B